

Article

Impact of Wave Energy Converters and Port Layout on Coastal Dynamics: Case Study of Astara Port

Mehrdad Moradi * and Adrian Ilinca *

Department of Mechanical Engineering, University of ETS (École de Technologie Supérieure), 1100, Rue Notre-Dame Ouest, Montréal, QC H3C 1K3, Canada

* Correspondence: mehrdad.moradi.1@ens.etsmtl.ca (M.M.); adrian.ilinca@etsmtl.ca (A.I.)

Abstract: In the face of depleting fossil energy and the imperative of sustainable development, there is a compelling drive towards advancing renewable energies. In this context, sustainable and predictable alternatives, like marine energy, gain prominence. Marine energy presents a cleaner option devoid of the adverse effects associated with fossil fuels, playing a crucial role in environmental sustainability by safeguarding coastlines against erosion. This study focuses on Astara Port in the Caspian Sea, exploring the utilization of wave energy converters (WECs). The originality of this study's research lies in exploring WECs' dual role in energy generation and coastal protection. Using MIKE21 software simulations, the impact of number, location, arrangement, and orientation of WECs across various scenarios was investigated, including two WEC number scenarios (11 and 13), three structural placement scenarios (north, front, and south of the port), two structural arrangement scenarios (linear and staggered), two port layout scenarios (original layout and modified layout), and two orientation scenarios for the structures (facing north-east, which is the dominant wave direction, and facing southeast). The results show a remarkable decrease in the significant wave height behind WECs, notably with 13 staggered devices facing dominant waves (from northeast), reducing the significant wave height H_s by 23–25%. This setup also shows the highest wave height reduction, notably 36.26% during a storm event. However, linear WEC setup offers more extensive coastline protection, covering 47.88% of the model boundary during storms. Furthermore, the 11 staggered WECs facing southeast (SE) arrangement had the lowest sediment accumulation at 0.0358 m over one year, showing effective sedimentation mitigation potential. Conversely, the 13 linear WECs facing northeast (NE) had the highest accumulation at 0.1231 m. Finally, the proposed port design redirects high-velocity flow away from the port entrance and removes rotatory flow, reducing sediment accumulation near the harbor entrance.



Citation: Moradi, M.; Ilinca, A.

Impact of Wave Energy Converters and Port Layout on Coastal Dynamics: Case Study of Astara Port. *Energies* 2024, 17, 2485. <https://doi.org/10.3390/en17112485>

Academic Editors: Umesh A. Korde and Michael E. McCormick

Received: 18 April 2024

Revised: 19 May 2024

Accepted: 20 May 2024

Published: 22 May 2024



Copyright: © 2024 by the authors. Licensee MDPI, Basel, Switzerland. This article is an open access article distributed under the terms and conditions of the Creative Commons Attribution (CC BY) license (<https://creativecommons.org/licenses/by/4.0/>).

1. Introduction

In pursuing Sustainable Energy Development, a pivotal consideration lies in substituting fossil fuels with a myriad of renewable energy sources. This imperative has led to an escalating demand for the augmentation of renewable energy production. Within the spectrum of renewable energy generation methodologies, wave energy production emerges as an up-and-coming option due to the high density of water, the predictability of waves, and the minimal environmental footprint. Despite its immense potential, wave energy is still in its infancy, necessitating further in-depth research and substantial investment to establish it as a dependable and recognized source of energy production in the scientific and technological domain [1].

Numerical and experimental studies have delved into this energy source, revealing its potential for sustainable and reliable energy production and its role in safeguarding coasts and ports from erosion, sedimentation, and storms [2–5].

Wave energy converters (WECs) are key players in emission reduction efforts. They generate clean electricity from renewable ocean waves, helping to reduce our dependence on fossil fuels and their associated emissions. WECs offer a low carbon footprint and minimal environmental impact compared to traditional power plants, preserving marine ecosystems while diversifying our energy mix. In a recent study, Choupin et al. [6] analyzed wave energy converters' role in reducing emissions. They introduced a process for optimal converter-location pairs, considering various factors. The study in Southeast Australia highlighted spatial variations in nearshore pairs and introduced an Index to rank areas based on their energy demand.

Given the hefty costs tied to wave energy converter (WEC) development, numerical simulation is vital for refining design precision and deployment strategies, leading to cost-effective modeling of renewable wave energy. Smith et al. [7] employed numerical wave models and adapted SWAN codes to evaluate the influence of offshore wave farms on the nearby wave climate. Their findings demonstrate the correlation between the extent of the impact and the response characteristics of the devices, as well as the spectral sea state under consideration. In another study, the SWAN coastal model was used to investigate the impact of WEC arrays on surrounding wave conditions. The results showed that WEC arrays could create wakes up to 200 m behind, reducing estimated power performance by 2.3% to 6.0% [8].

Physical modeling of WECs through scaled prototypes in controlled environments offers insights into real-world performance and helps optimize design for increased efficiency and reliability. Through physical model tests, Ruol et al. [9] explored the efficiency and transmission characteristics of the DEXA wave energy converter, investigating its potential dual applications. They proposed deploying a DEXA array in Marina di Ravenna to evaluate its impact on longshore sediment transport, possibly reversing the net transport direction. The study concluded that a WEC farm reduces coastal wave energy, significantly affecting sediment transport. Nader et al. [10] introduced a new experimental method for studying WEC arrays, overcoming cost and complexity barriers. They aimed to understand array performance and develop accurate modeling techniques. Initial results showed promising insights into array hydrodynamics, suggesting potential design improvements.

The distance between a wave farm and the coast significantly influences energy production and environmental effects. Optimal placement of WECs involves considering factors such as wave resource availability, transmission losses, and ecological and environmental effects. Abanades et al. [11] examined the influence of the distance between a wave farm and the coast. Their study, conducted in Perranporth (UK), revealed that the closest farm offers the most significant protection, resulting in up to a 20% reduction in erosion. However, this proximity entails a minor trade-off, leading to a slightly smaller wave resource by approximately 10%.

The Wave Dragon is a Wave Energy Converter (WEC) designed to harness energy through overtopping. It captures energy primarily by directing waves onto a ramp and into a reservoir and a set of Kaplan turbines; some studies have investigated the mechanism of this type of WEC in detail [12–18]. Robertson [19], in a study, compared the Wave Dragon Over-Topping Device and the Pelamis for deployment along the coasts of Vancouver Island and the Queen Charlotte Islands. Results showed that both devices have promising capacity factors: Pelamis achieved 51% on Vancouver Island and 59% on the Queen Charlottes, while Wave Dragon reached 21% and 30%, respectively. This suggests significant opportunities for efficient renewable wave energy generation in these regions. In another study, Iglesias et al. [20] investigated how the distance of a wave farm from the coast affects nearshore wave conditions. They used case studies with varying distances (2 km, 4 km, and 6 km) and wave conditions. The study results showed that increasing the distance from the coast doesn't consistently reduce the Maximum absolute Nearshore Impact, and the distance influences where the maximum impact occurs along the coast. Extensive laboratory testing on a scale model of a Wave Dragon energy converter was conducted from 1998 to 2001 at Aalborg University [21], leading to the creation of a 57 × 27 m prototype in Nissum

Bredning, Denmark, which became the world's first offshore wave energy converter in May 2003. Kofoed et al. [22] concluded that the turbines face three main challenges: operating at low head values (0.4 to 4.0 m), dealing with frequent regulation due to wave overtopping variations and limited storage, and operating in a harsh environment with minimal maintenance on an unmanned offshore platform.

Nørgaard et al. [23] conducted experimental investigations using a 1:51.8 scale physical model of the 260×150 m, 24 kW/m model Wave Dragon device. Their study also examined the influence of the Wave Dragon's mooring system and reflector joints on wave height reduction and transmission.

Given the significance of waves, their influence on coastal areas, and their considerable energy generation potential, this study utilizes numerical modeling to examine the impact of Wave Dragon devices on nearshore wave and flow characteristics. The innovation of this study stems from exploring the dual role of WECs in energy generation and coastal protection, comparing linear and staggered arrangements, analyzing orientation effects, and proposing a novel port design for sedimentation management to move it away from the port entrance. Various scenarios are being investigated to simultaneously achieve coastal protection and maximize energy generation. Reducing wave height can mitigate coastal erosion and facilitate energy dissipation by the WECs, with the dissipated energy being convertible to electricity.

2. Materials and Methods

This research used the two-dimensional hydrodynamic model MIKE21 2024 software and its subsets to model the wave and flow patterns in the study area. The model uses wind speed, wind direction, wave height, wave period, and bed topography as meteorological, hydrodynamic, and geographical input data. This investigation delves into examining Astara Port in the Caspian Sea. It underscores the port's significance and the critical need to prevent coastal erosion and sedimentation in its vicinity. Furthermore, the study explores the feasibility of harnessing wave energy for electricity generation. It is worth noting that the methodology employed in this investigation is transferable to similar ports facing comparable challenges. In future studies, using Boussinesq-type equation models and software like MIKE21 could be beneficial for simulating hydrodynamic conditions and sediment transport in offshore, coastal, and harbor areas [24,25].

2.1. MIKE21 Mathematical Model

For the analysis of marine phenomena, the MIKE21 model is one of the most practical models developed by the Danish Hydraulic Institute (DHI). MIKE21 is a suitable tool for analyzing phenomena such as wave pattern, current, sedimentation, determination of sediment transport rate, wind-generated waves, and specific shallow water (SW) processes such as wave breaking, erosion, and bed effect [26].

The mathematical equations used in the SW module are the equations of equilibrium density of the wave spectrum, which are solved in the frequency range of the wave's zero-order and first-order energy spectra using the finite difference method and ADI (Alternating Direction Implicit) technique [27].

$$\frac{\partial(c_{gx}m_0)}{\partial x} + \frac{\partial(c_{gy}m_0)}{\partial x} + \frac{\partial(c_gm_0)}{\partial \theta} = S_0 \quad (1)$$

$$\frac{\partial(c_{gx}m_1)}{\partial x} + \frac{\partial(c_{gy}m_1)}{\partial x} + \frac{\partial(c_gm_1)}{\partial \theta} = S_1 \quad (2)$$

Here, m_0 and m_1 are zero and first-order momentums, respectively; C_{gy} and C_{gx} are wave group velocity components; S_1 , and S_0 are energy sources, which can be increased by

wind, or decreased by energy dissipation due to bed friction and wave break. In the above equations, $m_n(\theta)$ can be calculated using Equation (3):

$$m_n(\theta) = \int_0^\infty \omega^n A(\omega\theta) d\omega \quad (3)$$

where ω is the frequency, and A is the wave power spectrum density. For hydrographic maps used in the SW module, the ratio of the distance of the computational nodes in the y and x directions and the maximum angle between the direction of the propagated wave on the x -axis are of great importance. These criteria are determined as follows:

$$\frac{\Delta x}{\Delta y} \geq 4 \quad (4)$$

The maximum angle between the wave propagated direction and the x -axis must not exceed $\pm 60^\circ$.

The SW module simulates the wave-breaking phenomenon based on the proposed relations of [28].

$$\frac{dE}{dt} = -\frac{\alpha}{8\pi} Q_b \omega H_m^2 \quad (5)$$

$$\frac{1 - Q_b}{\ln Q_b} = -\left(\frac{H_{rms}}{H_m}\right)^2 \quad (6)$$

$$H_m = \gamma_1 k^{-1} \tanh\left(\frac{\gamma_2 kd}{\gamma_1}\right) \quad (7)$$

where ω is frequency, H_{rms} is the square root of the average squares of wave height, H_m is the maximum allowable wave height, Q_b is friction due to wave breaking, which affects energy dissipation rate, k is wave number, d is water depth, α is the energy dissipation coefficient, γ_1 is a constant coefficient controlling critical wave rise, and γ_2 is a constant coefficient controlling the critical water depth.

Hydrodynamic models can calculate wave refraction, shoaling, wave break, radiation stresses, wave setup, and the velocity of parallel currents on the shore. Wave characteristics, including wave height, wave period, and mean wave direction, are used as time series. The hydrodynamic model operates by numerically solving the two-dimensional shallow water equations. This includes solving continuity, momentum, temperature, salinity, and density equations. The model uses both Cartesian and spherical coordinates for the horizontal domain. Here, the governing equations of hydrodynamic models are not presented due to document limitations. Additional information is available in [28].

2.2. Problem and Solution

Given the common challenges encountered by coastal regions worldwide, including the pressing issue of coastal erosion, it remains crucial to formulate prompt and practical solutions. According to the analysis of the region's wave and wind climate, it was concluded that erosion problems exist in the southern parts of Astara Port. However, the sediment accumulation problem at the port entrance is more severe. This accumulation leads to the closing of the harbor with sand washed away from the northern parts of the port. The main problem is keeping the port from being sealed off by accumulating sand. The sand must be removed from the harbor entrance and transferred into the natural longshore sediment transport system. This is usually done through a dredging operation, which requires much effort and is expensive. Figure 1 shows the existing erosion and sedimentation patterns in the southern and northern parts of the port, respectively. This problem exists in most ports around the world, and if a solution can be identified in this region, it would have positive outcomes for addressing similar issues in ports across the globe.

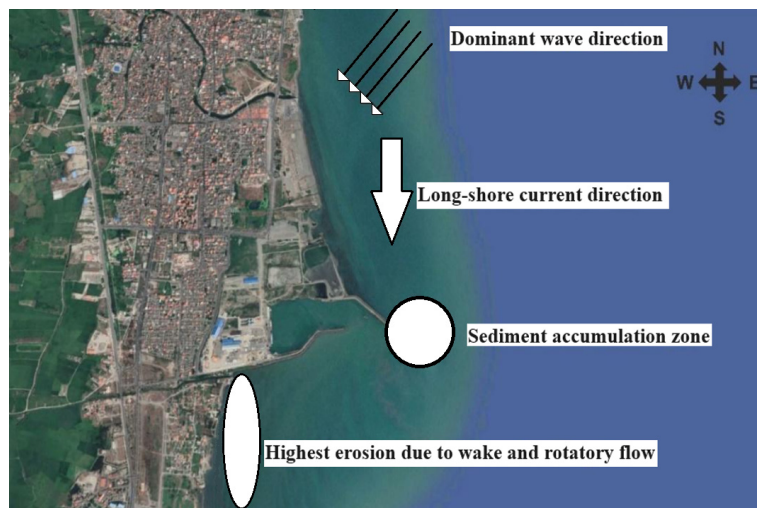


Figure 1. Erosion and sedimentation pattern near Astara Port.

As mentioned earlier, the erosion in the southern part of the port, as illustrated in Figure 1, is problematic and necessitates proactive intervention. It is crucial to address this issue because it can potentially jeopardize the stability of the breakwater structure, which, in turn, is instrumental in maintaining a stable flow pattern near the port. Figure 2 shows the transition of the coastline in the southern part of the port over nine years, from 2012 to 2021. In this figure, the white line represents the coastline in 2021, while the yellow line corresponds to the coastline in 2012. It is evident from this comparison that erosion poses a substantial and immediate threat to the properties and stability of the southern areas within the port.

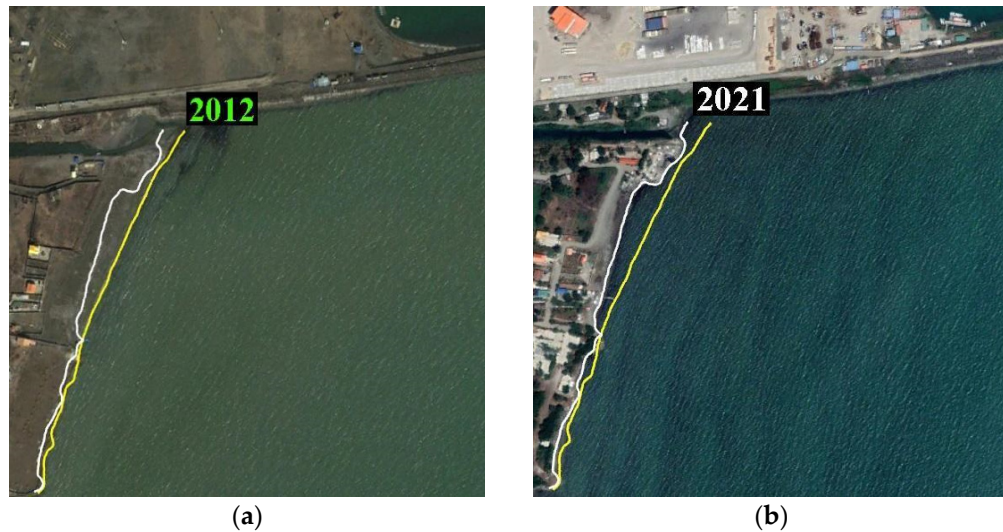


Figure 2. Coastline transition from (a) in 2012 to (b) in 2021.

2.3. Experimentally Recorded ADCP (Acoustic Doppler Current Profiler) and Bathymetry Data

The calibration of the MIKE21 wave and current model constants requires experimental data. These data include the speed and direction of the flow, height, and wave direction at different points. The following section describes the available data used in these studies. Simulation studies of the northern coasts of Iran near Astara Port have involved several measurements in the South Caspian Sea. On the coast of Astara Port, flow features were measured in 2013 at depths of 10 and 25 m [29]. This study uses an Acoustic Wave and Current profiler (AWAC) device for current measurement and wave recording (Figure 3).

Using this device, it is possible to accurately record waves and flow details and calibrate the MIKE21 model.



Figure 3. Acoustic Doppler profiler used for recording experimental data [30].

2.4. Global and Local Models Setup

To set up the model effectively, coastal geography and seabed topography are essential data. Additionally, comprehensive wind speed and direction statistics are vital, as they significantly influence wave patterns, coastal dynamics, and overall hydrodynamics. The wind data were obtained from ECMWF (European Centre for Medium-Range Weather Forecasts). According to these data, the dominant wind direction is from northeast to southwest, the same as the dominant wave direction. To simulate the flow and wave using the global model, an unstructured meshing system was used in the deep-water area, and rectangular grids were used in the southern regions. In the initial stages of configuring the local model, the first step involves furnishing the model with the mesh domain.

Given that this study centers around examining Astara Port, the local model is specifically tailored to the vicinity of the port. Defining the borders of the local model is determined by the project's specific requirements. Once the global model has been calibrated and executed, boundary conditions are extracted from the global model's outputs along the borders of the intended local model. This extraction process is facilitated using the Data Extraction FM tool within MIKE Zero. Figure 4 illustrates the boundaries of the global and local models, their mesh structures, and contours of bathymetry values.

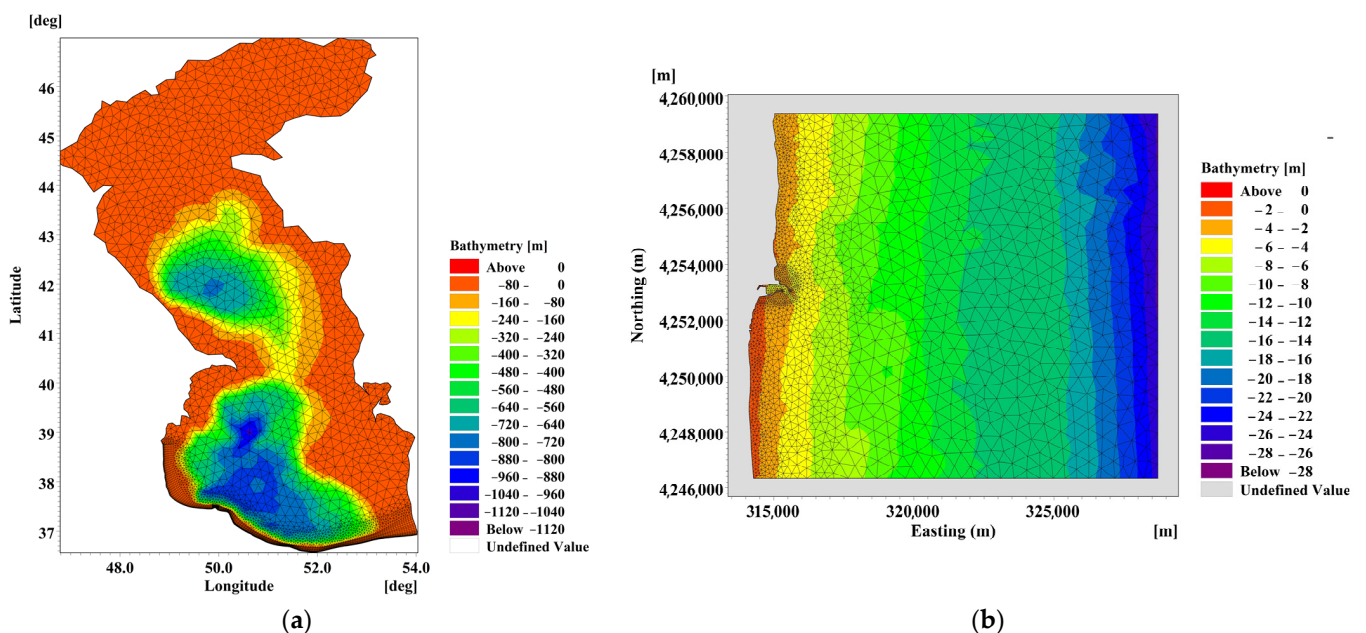


Figure 4. Boundaries and mesh grids of the (a) global model and (b) local model.

2.5. Outputs of the Local Model

The results generated by the MIKE21 local model are validated with experimental data, encompassing variables like flow velocity, flow direction, wave height, and wave direction. It is important to note that the accuracy of the two-dimensional model in predicting flow along the Astara shores is notable due to its ability to calculate the simultaneous influence of both wind and waves. Moreover, the model's simultaneous calculation of both wave and current variables highlights the importance of precise wave feature prediction. As mentioned, ADCP devices were utilized to measure the characteristics of waves and currents at depths of 10 and 25 m near Astara Port. These two points were used to validate the model values (Figure 5).

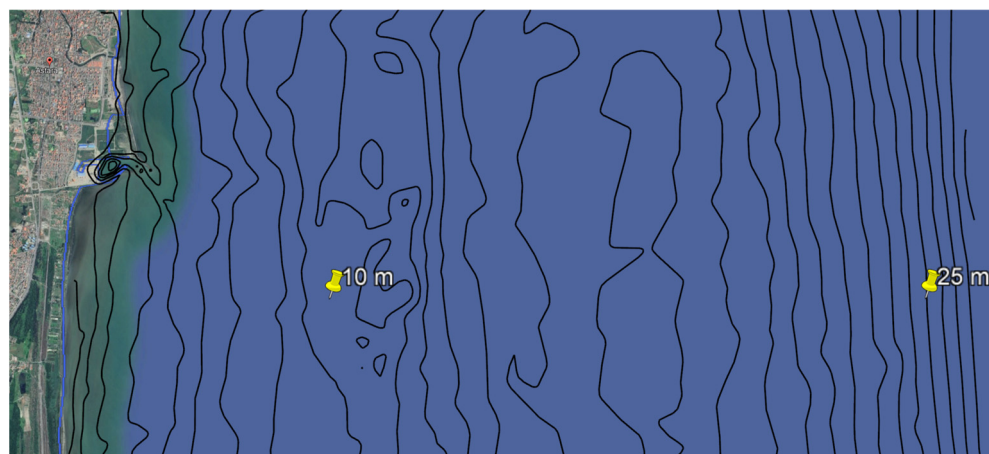


Figure 5. The exact location of flow and wave measurements.

The local model was established, and the simulations near the port were performed using the global model results. Figure 6 shows wave characteristics for one year's modeled and measured data. Figure 7 compares measured and modeled depth-averaged current velocity and flow direction in 2013 at the 10 m depth station. As evident in Figures 6 and 7, current and wave results across the 10 m station suggest that the model's predictions for coastal regions are reasonably accurate, especially for the storm events in the region throughout the year.

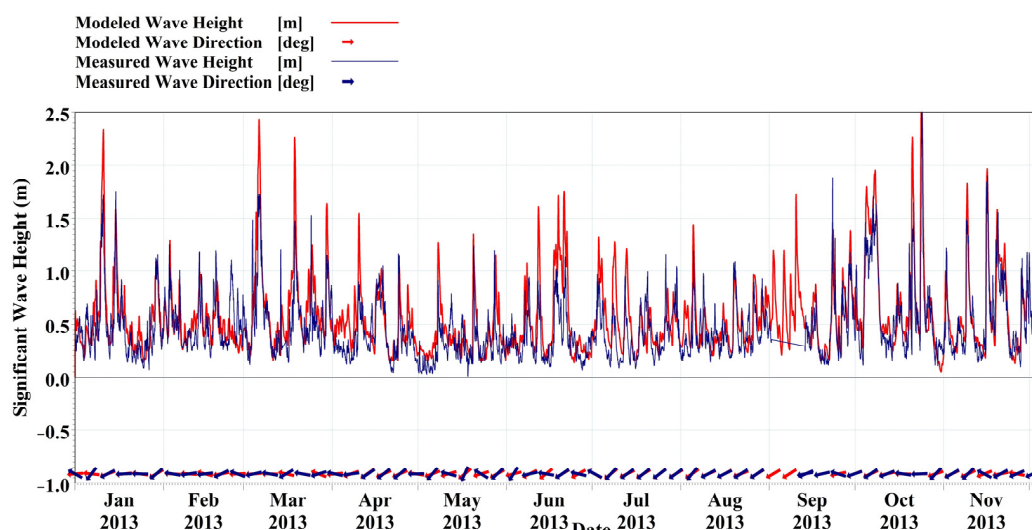


Figure 6. Validation of the Spectral Wave (SW) local model using modeled data and measured data at the Astara 10 m station.

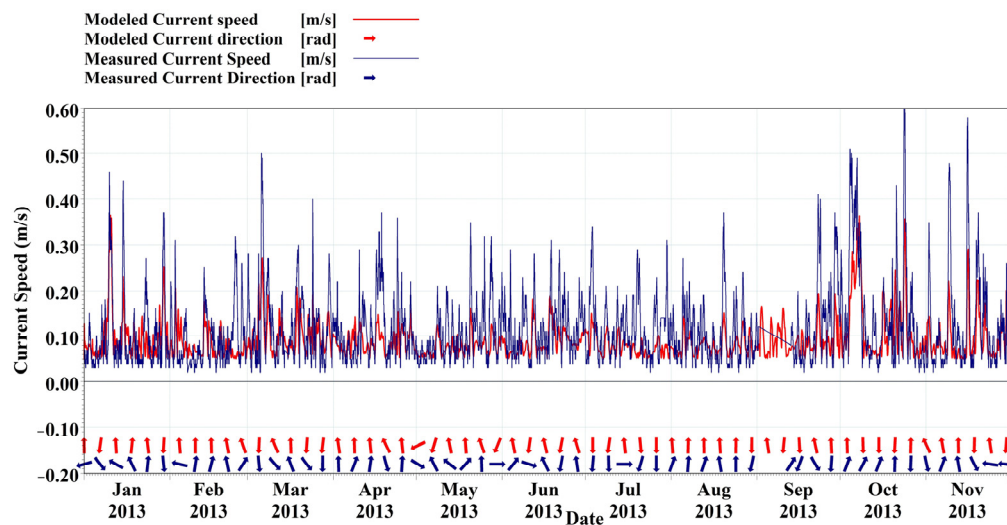


Figure 7. Measured and modeled flow direction and velocity at the Astara 10 m station.

2.6. WEC Type, Placement and Orientation

In the pursuit of achieving outcomes, including erosion control and generating electricity, strategic positioning of WECs was executed. Wave Dragon overtopping devices were used in this study. They are controlled using a mooring system and have six degrees of freedom in the real world. However, due to limitations in the modeling of moving objects within the MIKE21 software and the relatively small movements compared to the scale of the global and local models used in this study, wave energy converters (WECs) are considered static. The device employed in this study is a 76×50 m, 12 kW/m model Wave Dragon device that uses wave reflectors to direct waves up a ramp into a reservoir; the stored water then flows through turbines to generate electricity (Figure 8).

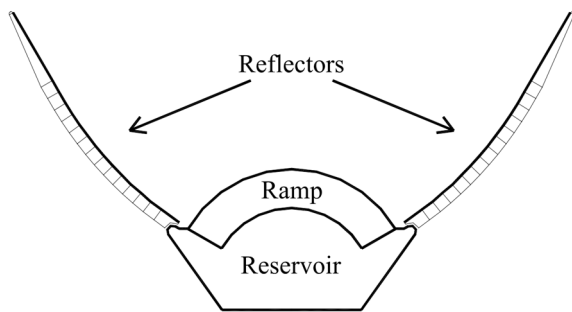


Figure 8. The basic layout of the Wave Dragon energy converter [31].

Testing various scenarios was necessary to maximize wave capture, electricity generation, and energy dissipation to combat coastal erosion. This involved exploring different WEC numbers and arrangements within the wave farm, adjusting the wave farm's location, and modifying the port design. The objective is to optimize energy generation efficiency, protect the coastline, and minimize sedimentation at the port entrance, reducing the need for costly operations like dredging.

In general, the simulations were performed for two WEC number scenarios, 11 and 13; two arrangement scenarios, linear and staggered; two scenarios for the orientation of WECs facing north-east (dominant wave direction) and facing southeast; three wave farm placement scenarios: north, front, and south of the port; and two port layout scenarios: original layout and modified layout (Table 1).

Table 1. Simulation Scenarios for Wave Energy Converters (WECs).

Simulation Parameters	Scenarios
WEC Number	11, 13
Arrangement	Linear, Staggered
WEC Orientation	NE (Northeast) and SE (Southeast)
Wave Farm Placement	North, Front, and South of the port
Port Layout	Original, Modified

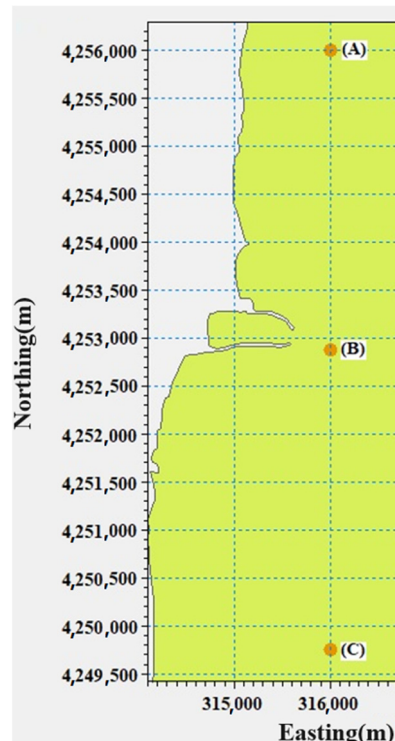
For example, 13 Linear NE-Front of the modified port describes a simulation with 13 linearly arranged WECs facing northeast and placed at the front of the modified port layout.

3. Results

This section investigates the impact of different scenarios on wave characteristics and sedimentation. To this end, time-averaged point analysis, linear analysis, and aerial data are studied to comprehensively assess how different implementation scenarios affect wave behavior and sedimentation processes.

3.1. Time-Averaged Wave Height of Different Points

To assess the influence of structures on significant wave height (H_s), an investigation was conducted at three designated locations in the northern (A), frontal (B), and southern (C) parts of the port. Subsequently, the H_s values were extracted at these specific points over three consecutive months (January to March). Figure 9 provides a depiction of the geographical location of these identified locations. Additionally, these points were studied for different scenarios involving the location, orientation, arrangement, and number of WECs. When comparing the no-structure scenario with other scenarios, the analysis reveals a clear reduction in significant wave height around the wave energy converters.

**Figure 9.** Location of the three points studied on the North (A), Front (B), and South (C) of the port.

Regarding the impact of WECs across various scenarios, Figures 10–12 show that configurations featuring 13 structures oriented towards the northeast with a staggered layout exhibit the most effective reduction in wave height. Following this, scenarios involving 13 structures arranged linearly demonstrate comparatively favorable results. Conversely, configurations comprising 11 staggered structures facing southeast exhibit the least pronounced impact on wave height reduction across all scenarios evaluated.

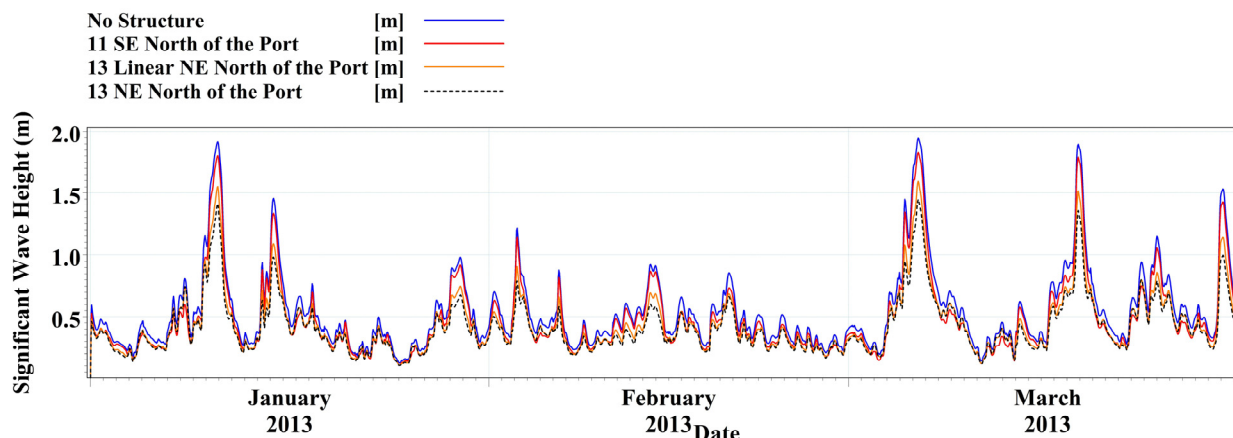


Figure 10. Significant wave height (H_s) in point (A) for various scenarios.

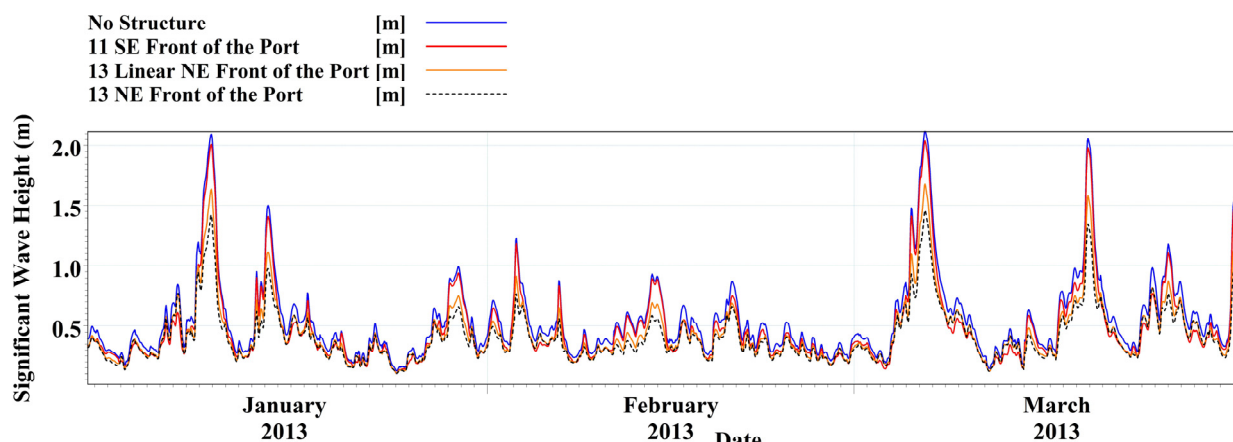


Figure 11. Significant wave height (H_s) in point (B) for various scenarios.

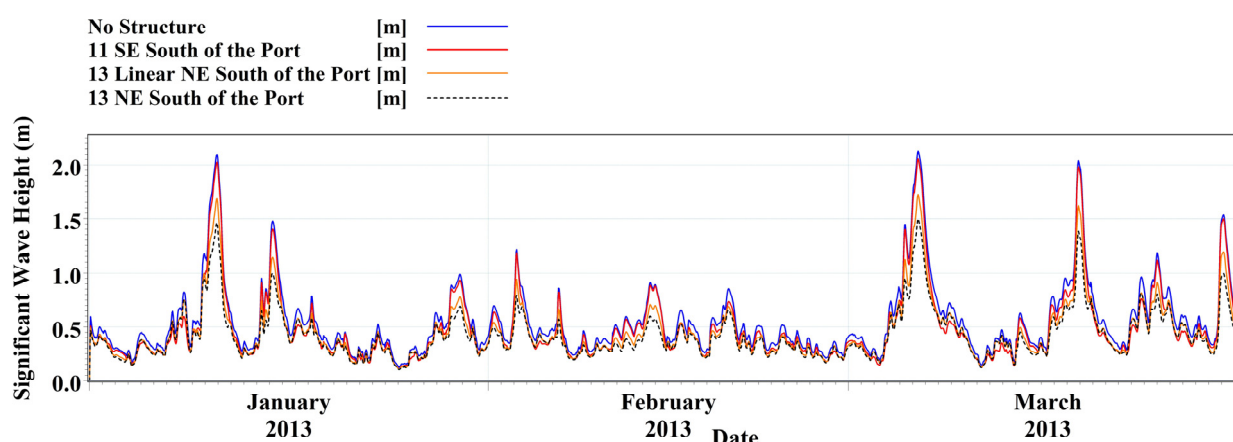


Figure 12. Significant wave height (H_s) in point (C) for various scenarios.

Following a thorough analysis of the time-averaged results for each of the points above, the data reveal significant decreases in wave height across some scenarios of placements of WECs. Specifically, the simulations involving 13 staggered devices show 23.71%, 25.3%, and 23.57% reductions for points A, B, and C (north, front, and south WEC locations), respectively. For configurations featuring 13 linear wave energy devices, the corresponding reductions were 19.31%, 19.91%, and 18.08% for points A, B, and C, respectively. In the case of 11 staggered devices, the reduction values in wave height were 12.29%, 12.46%, and 12.02% for the points on the north, front, and south of the port, respectively. These substantial impacts on the wave height reduction show mitigation of erosion behind the Wave Energy Converters, particularly in the case study involving 13 staggered energy converters facing the dominant wave direction. This configuration resulted in an approximate 23% to 25% decrease in H_s values, indicating notable effectiveness in wave height reduction and erosion control measures.

3.2. Line Series to Assess the Impact of WECs on H_s along the Coastline

To further evaluate the impact of WECs along the coastline, the MIKE21 linear data extraction tool was employed. Data were extracted for a line parallel to the coastline at position 316,000, focusing on the modified port configuration during a storm event. The exported data included three WEC location scenarios (north, front, south) and three arrangement scenarios (staggered 13 NE, linear 13 NE, staggered 11 SE). The objective was to determine which scenario led to a more significant wave height (H_s) reduction in a line with identical water depth. The results are depicted in Figure 13 for three cases of devices installed to the (a) north, (b) front, and (c) south of the port. In these diagrams, the x-axis illustrates the distance from the southernmost point on the investigated line along the coast, and the y-axis corresponds to significant wave height values. It is evident from the diagrams that all three structure arrangements had a notable impact on wave height compared to the no-structure case.

Furthermore, the staggered arrangement in the 13 NE direction showed the highest decrease in significant wave height by 29.74%, 36.26%, and 31.86% when installed to the north, front, and south of the port, respectively. This proves that the maximum wave height reduction is observed when the WEC farm is in front of the port and staggered with the arrangement of 13 NE. The values of maximum wave height reduction for 13 NE linear are 22.75%, 29.62%, and 25.76% for north, front, and south of the port installation locations, respectively, and 26%, 17.1%, and 31.92% for 11 staggered devices to the north, front, and south of the port, respectively.

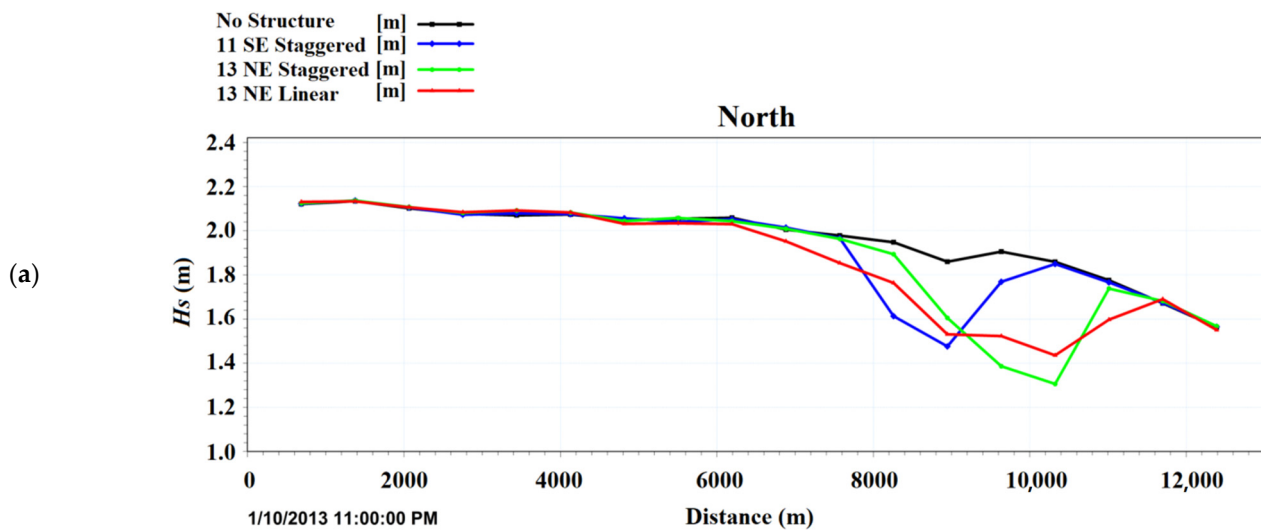


Figure 13. Cont.

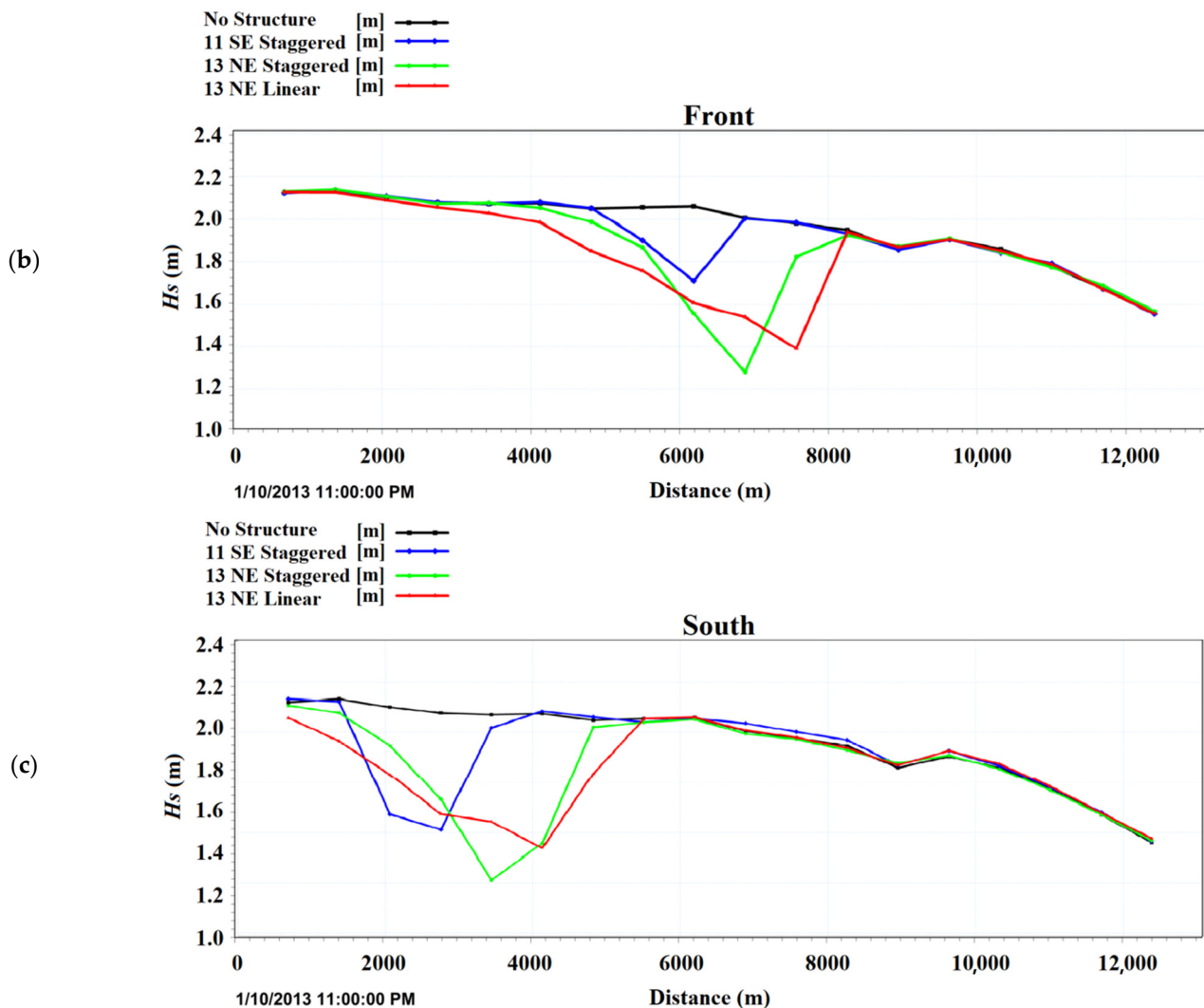


Figure 13. Line series of wave height for a line parallel to the coastline during a storm event for WECs located to the (a) north, (b) front, and (c) south of the port.

The data indicate that the 13 staggered arrangement facing northeast achieves the highest decrease in significant wave height during a storm across all placements. Specifically, the front placement scenario shows the most significant reduction, with a decrease of 36.26%. Therefore, it can be concluded that the optimal configuration for reducing significant wave height is 13 NE staggered, particularly when installed in front of the port.

However, the 13 NE linear arrangement demonstrated a broader length of effect (Figure 13), indicating superior performance in mitigating wave height across a wider region. The linear arrangement of WECs impacted 41.52%, 47.88%, and 46.6% of the total length of the local model boundaries for the north, front, and south of the port placements, respectively. For the 13 staggered WECs, these percentages were 35.59%, 35.84%, and 27.11% for the north, front, and south scenarios, respectively. Finally, the reduction percentages for the 11 staggered devices were 22.88%, 17.79%, and 21.18% for north, front, and south, respectively. The percentages show that linear arrangements tend to cover a larger portion of the coastline compared to staggered configurations, indicating potentially greater effectiveness in influencing wave heights and mitigating coastal erosion over a broader area. The highest percentage (47.88% length of the local model boundary), indicating the most significant coastline coverage, is observed for the front of port placement scenario. Therefore, it can be considered the optimum choice for the linear arrangement to maximize the coverage of coastline protection by WECs. These results suggest that the

choice of WEC farm arrangement and location plays a significant role in determining the extent of the coastline affected.

3.3. Effect of Different Arrangements, Orientation, and Location on Aerial Wave Height Reduction

The significant wave height contours under various scenarios of WECs placement, orientation, and arrangement are depicted in Figures 14–16. As mentioned in the preceding section, the linear arrangement of WECs exhibits a broader impact on wave height across the area (Figure 14), whereas 13 staggered WECs oriented towards the northeast (Figure 15) demonstrate more significant reductions in wave height values within a smaller spatial extent. Additionally, the configuration involving 11 WECs facing southeast (Figure 16) has a marginal effect on wave height reduction. Furthermore, the southeast orientation of these WECs away from the dominant wave direction reduces their efficacy in power generation and wave capture.

Selecting the most suitable wave farm arrangement and location is crucial for each region's specific needs and the prevailing erosion patterns. In this case, both linear and staggered arrangements facing northeast have demonstrated acceptable efficiency in wave height reduction and erosion mitigation. Moreover, more significant wave height reduction by these structures implies increased energy dissipation, indicating higher potential for power generation, especially evident in this study for the 13 staggered devices facing northeast.

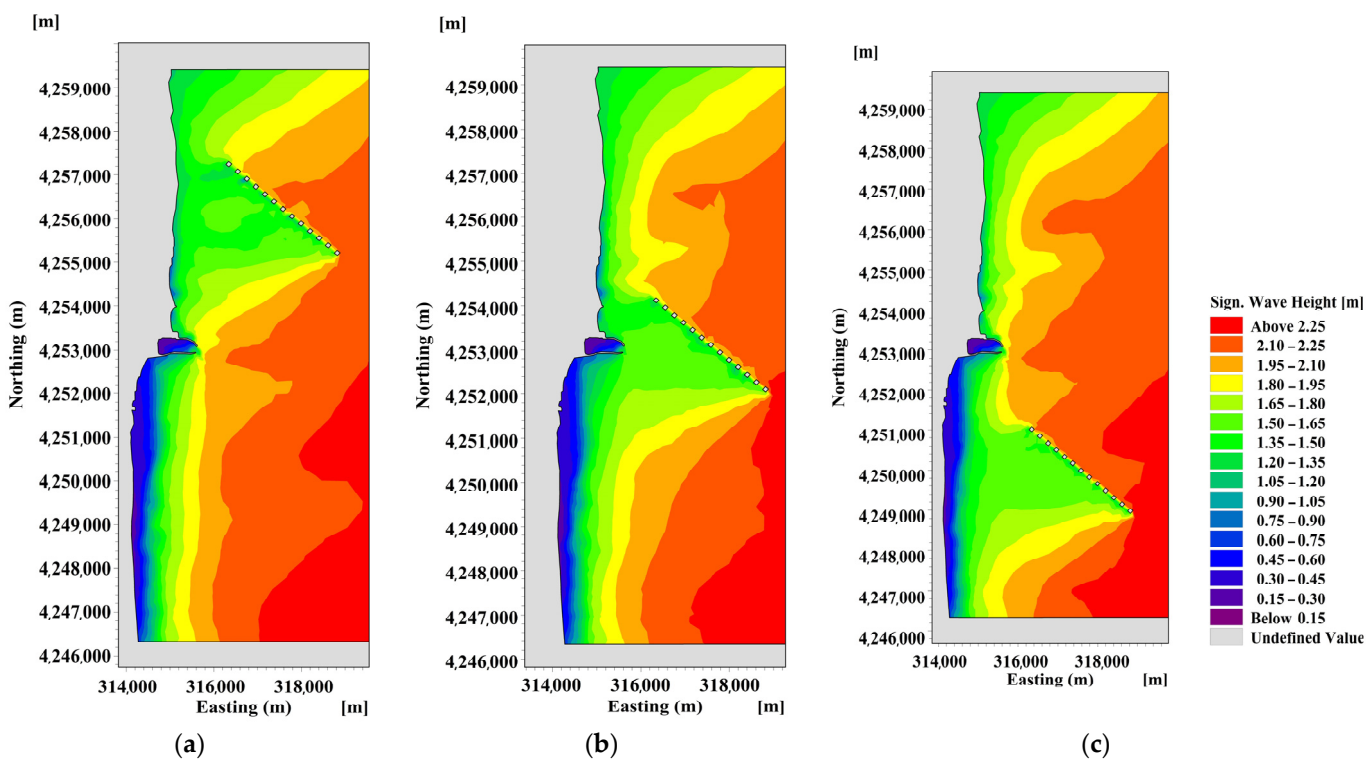


Figure 14. Wave height diagram in presence of 13 linear wave energy devices on (a) north; (b) front; and (c) south of the port.

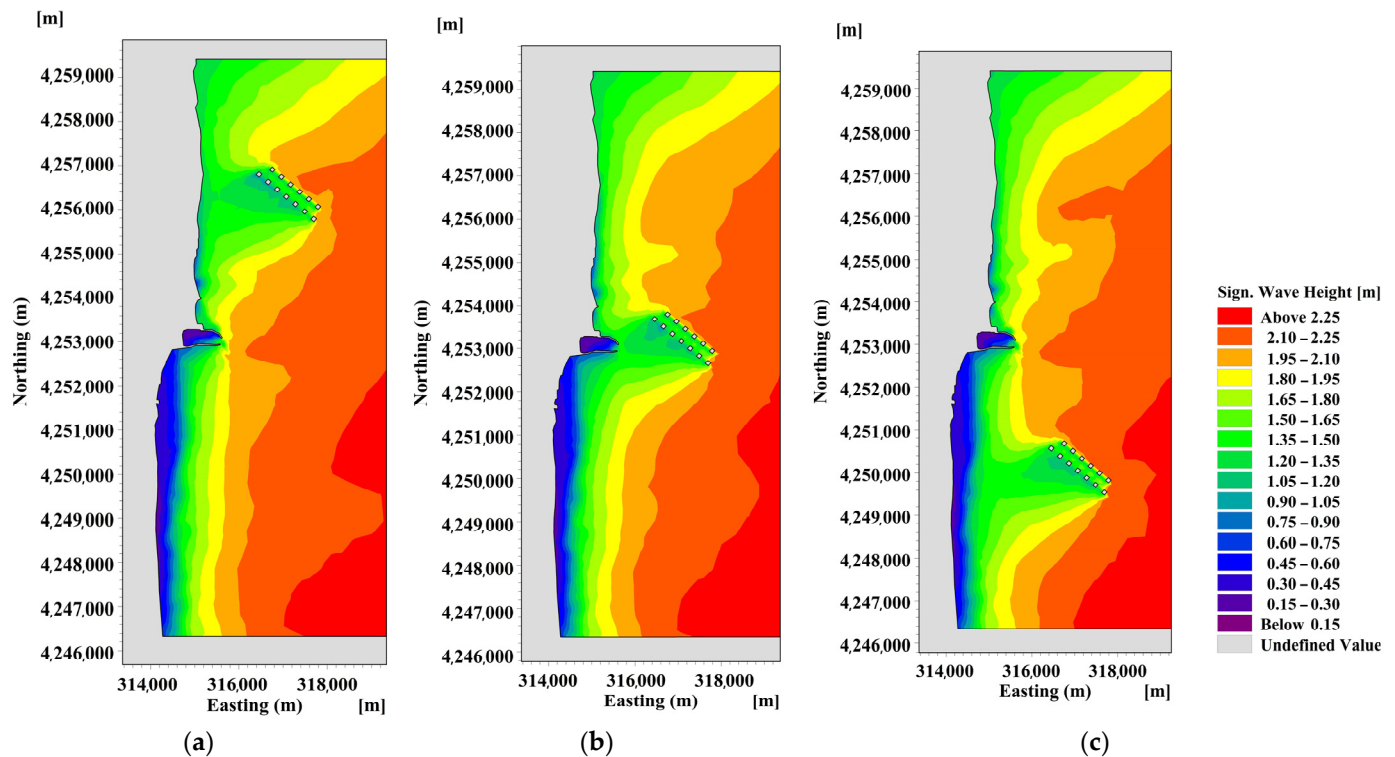


Figure 15. Wave height diagram in the presence of 13 staggered wave energy devices on (a) north, (b) front, and (c) south of the port.

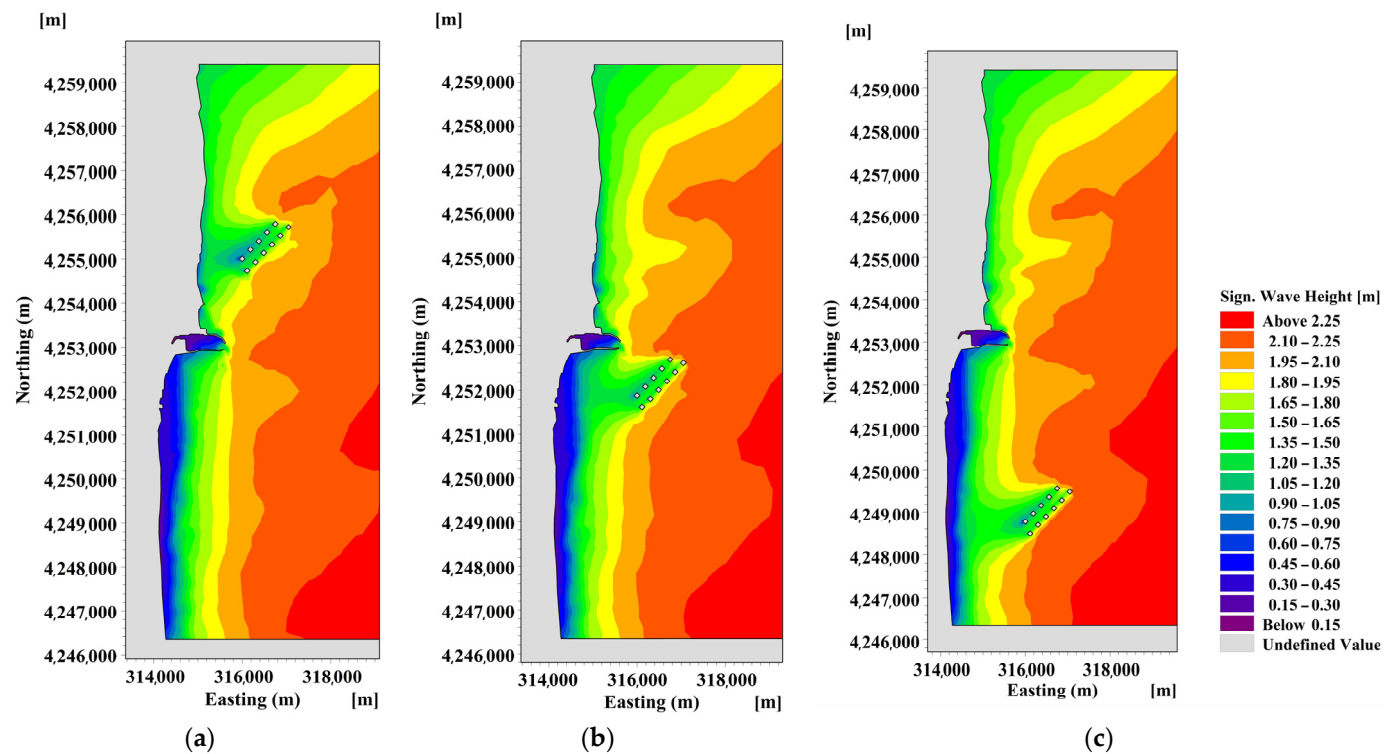


Figure 16. Wave height diagram in the presence of 11 staggered wave energy devices on (a) north, (b) front, and (c) south of the port.

3.4. The Impact of Harbour Layout on Near Port Current Speed and Sedimentation Pattern

The flow model (FM) and sand transport model (ST) were run for the year of 2013 using MIKE21 simulations to see the impact of placement of WECs in front of the port and port layout on sedimentation and flow pattern near the port entrance. The sediment transport model (ST) uses empirical equations to simulate sediment movement based on factors like grain size, sediment concentration, and flow velocity. On the other hand, the flow model (FM) relies on shallow water equations (Saint-Venant equations) to simulate water flow dynamics, considering factors such as water depth, flow velocity, and external forces like gravity and friction. As evident from the annual bed level change diagrams (Figure 17), there is a noticeable sediment deposition at the port entrance, which can have severe implications for commuting and the possibility of the port being closed due to accumulated sediments [32,33]. As the first step to preventing the port's closure and reducing sedimentation, wave energy converters were proposed and modeled in simulations. Results showed that wave energy devices do not provide a complete solution to eliminate the necessity for dredging and may even make the sediment accumulation issue more severe (Figure 18).

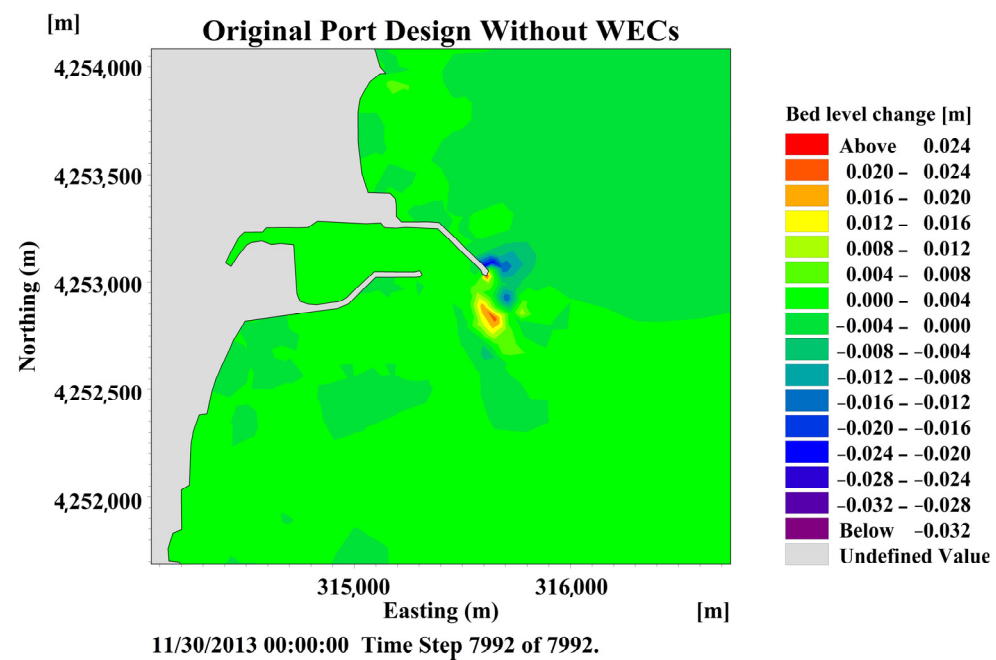


Figure 17. Sediment accumulation in the original port design.

Proposing a new design for the harbor was suggested to solve this problem. This modified design incorporates two curved arms that guide the high-velocity currents away from the harbor entrance. The intended outcome of this layout is a reduction in the formation of vortices and circular flows, which have been identified as the main reason behind the accumulation of sediment at the harbor entrance in the original layout of the port (Figure 19). Owing to this high-velocity flow passing by the port entrance without rotatory flow (Figure 20), sediment particles do not linger long enough to settle near the harbor opening. Instead, they are transported towards the port's southern reaches (the dominant flow direction of the region is north to south). Thus, sediment deposits (which were formerly located near the port's entry) have shifted to its southern portions (Figure 21).

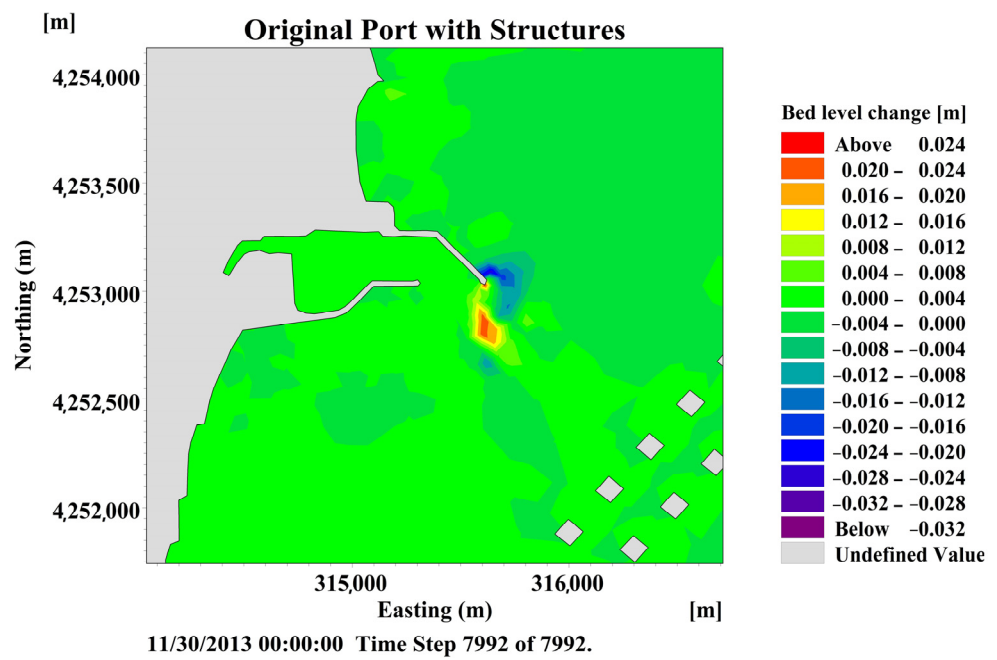


Figure 18. Sediment accumulation in the original port design in the presence of WECs in front of the port.

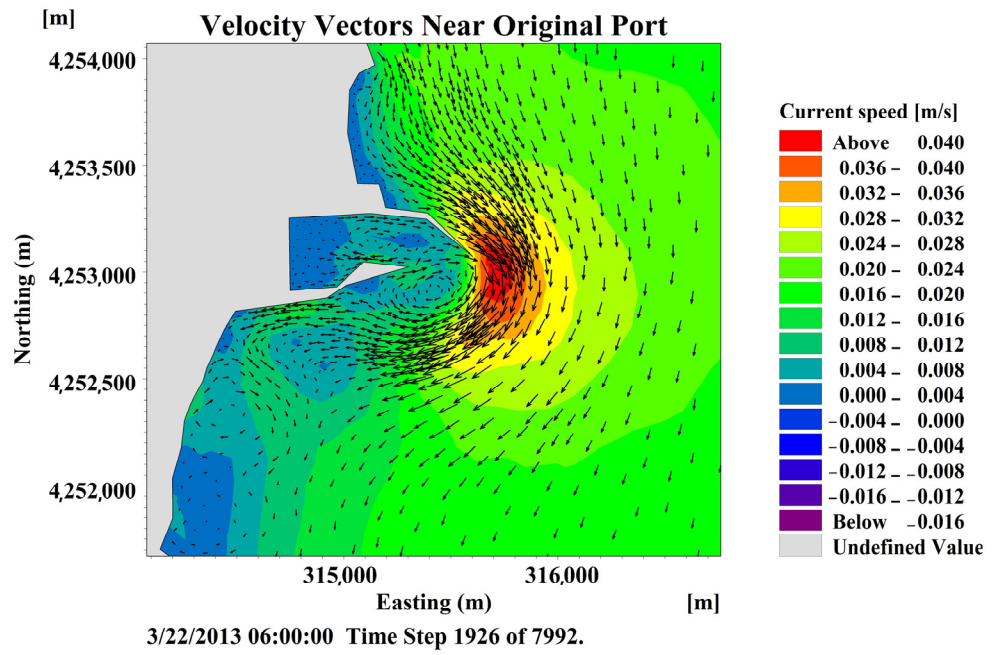


Figure 19. Velocity vectors and vortex formation near the original port layout.

Furthermore, the rotatory flow contributes to higher bed shear stress [34], thereby escalating erosion, especially notable in the southern regions of the original port layout. However, this rotatory flow has been eliminated in the modified port layout, reducing erosion in that part. These observations confirm that altering the flow dynamics can significantly impact sedimentation patterns, which in this case study results in a solution to the Astara Port entrance sediment accumulation problem and erosion issue. This can be utilized for ports with similar problems.

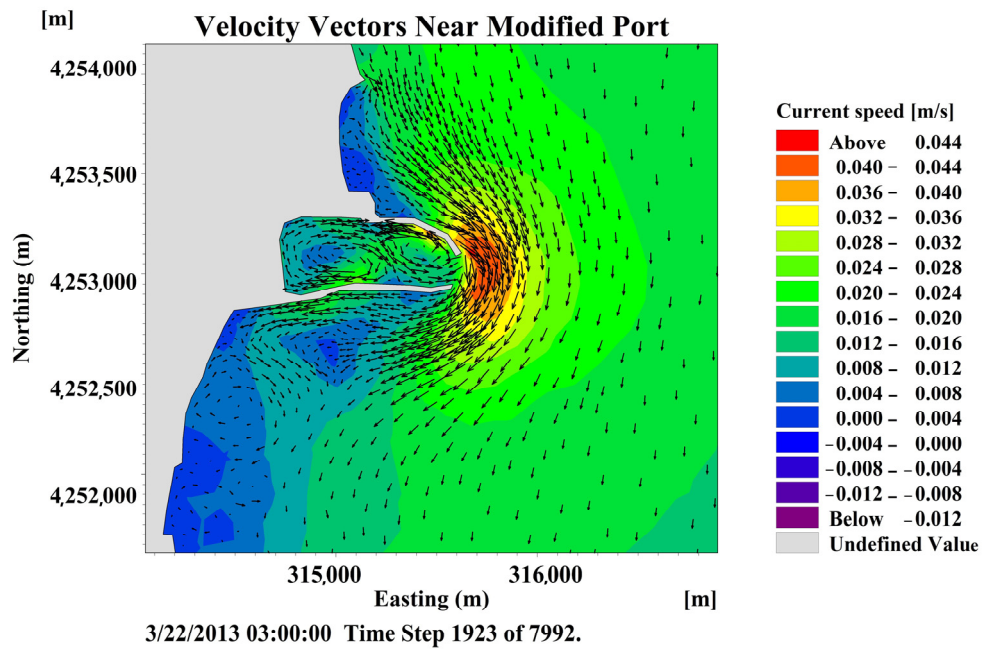


Figure 20. High-velocity flow passing by the port entrance of the modified port layout.

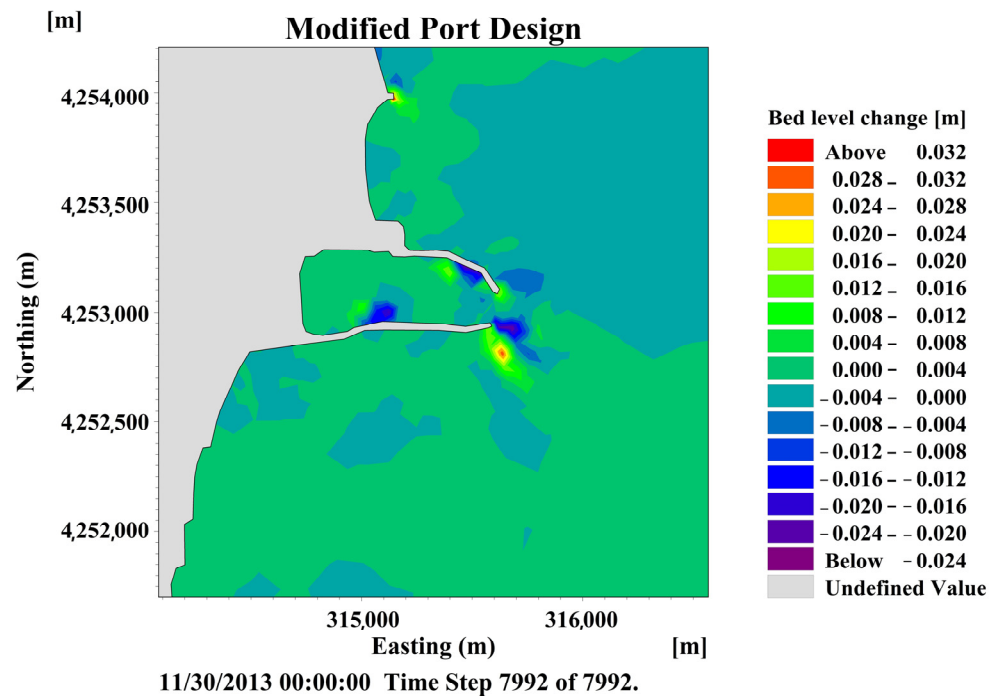


Figure 21. Annual bed level change south of the modified port layout.

The sediment accumulation near the port in 2013 was analyzed using the bed level change output of the MIKE21 ST (Sand Transport) model (Figure 22). This analysis included three different WEC arrangements: 11 SE staggered, 13 NE staggered, and 13 NE linear. By the end of the year, the sediment accumulation values for these scenarios were 0.0358 m, 0.0943 m, and 0.1231 m, respectively. The sediment accumulation analysis near the port indicates that the 11 SE staggered arrangement demonstrated the lowest sediment accumulation at 0.0358 m, indicating its good potential in mitigating sedimentation. Conversely, the 13 NE linear arrangement exhibited the highest sediment accumulation of 0.1231 m.

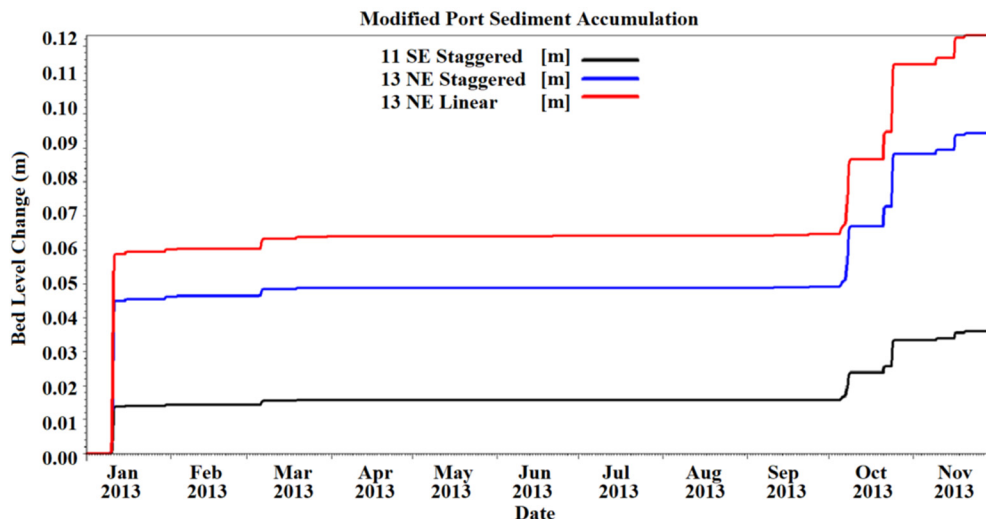


Figure 22. Comparison of the impact of different WEC arrangements on sediment accumulation downstream of the port.

4. Discussion

Waves are significant sources of energy that deform beaches and marine structures, carrying sediments along the shoreline (through longshore sediment transport) and perpendicular to the shore (through on-shore and offshore sediment transport). The main objective of this project is to achieve a stable pattern of how the waves operate around wave energy converters. The innovation of this study arises from examining the dual role of WECs in energy generation and coastal protection, comparing linear and staggered arrangements, analyzing WECs orientation effects, and proposing a novel port design for sedimentation management to move it away from the port entrance. Achieving the objectives of this study is feasible by recognizing the region's flow, wave, and wind pattern and studying the phenomena related to sea waves, such as wave height. These layouts were tested and simulated for both wave (SW) and flow (FM) models in 2013 and different scenarios.

The limitations of the MIKE21 2D model in capturing dynamic components highlight the need for future research to explore a 3D analysis of the flow field on a smaller scale. These studies should aim to investigate how Wave Energy Converters (WECs), specifically Wave Dragon devices, influence flow and wave dynamics as they move within the water. This shift to 3D analysis aims to provide a more comprehensive understanding of the interactions between WECs and the flow field, ultimately shedding light on their impact on coastal erosion and energy production potential. The necessity for this becomes more evident as many existing studies overlook the dynamic behavior of the Wave Dragon device by treating it as a static object and neglecting the modeling of mooring lines.

5. Conclusions

In studying the impact of WECs and port layout on flow hydrodynamics, sediment dynamics, and wave climate, different scenarios, including various locations of wave farms, the number of WECs, and their arrangement and orientation, were investigated. The result of this study demonstrates significant reductions in wave height, particularly notable in the case of 13 staggered energy converters facing the dominant wave direction, resulting in a 23% to 25% decrease in H_s values and effective erosion control. Moreover, among the configurations tested, the 13-staggered arrangement achieves the highest decrease in significant wave height during a storm event, especially evident in the front placement scenario with a reduction of 36.26%. This suggests that the optimal configuration for reducing wave height is the 13 NE staggered arrangement, particularly when positioned in front of the port. However, the linear arrangement of Wave Energy Converters (WECs)

offers better coastline protection coverage due to its extended impact length during storm events (47.88% of the length of the local model boundary).

These conclusions can be practically applied to real-world projects, especially those focused on coastal protection. The findings suggest that the 13 NE staggered arrangement of WECs, particularly when positioned in front of a port, is the most effective scenario in reducing wave height during storm events. The linear arrangement of WECs, despite providing less localized wave height reduction, offers broader coverage for coastline protection during adverse weather conditions. Integrating linear WEC arrangements into coastal protection projects can enhance overall coastal resilience by extending protection along a significant portion of the coastline.

Finally, the study proposes a new port design to address sediment accumulation, directing high-velocity flow away from the port entrance, effectively mitigating sediment deposition near the harbor opening. This redirection of flow results in sediment deposits shifting to the southern portions of the port, contributing to overall sedimentation control measures and improved port functionality.

Author Contributions: Conceptualization, M.M. and A.I.; methodology, M.M.; software, M.M.; validation, M.M. and A.I.; formal analysis, M.M.; investigation, M.M.; resources, M.M.; data curation, M.M.; writing—original draft preparation, M.M.; writing—review and editing, A.I.; visualization, M.M. and A.I.; supervision, A.I.; project administration, M.M. and A.I.; funding acquisition, A.I. All authors have read and agreed to the published version of the manuscript.

Funding: This research was funded by NSERC (Canada) through a discovery grant (grant number: RGPIN-2019-04220).

Data Availability Statement: The original contributions presented in the study are included in the article, further inquiries can be directed to the corresponding author.

Conflicts of Interest: The authors declare no conflicts of interest.

References

1. Falcao, A.F.D.O. Wave energy utilization: A review of the technologies. *Renew. Sustain. Energy Rev.* **2010**, *14*, 899–918. [[CrossRef](#)]
2. Clemente, D.; Rosa-Santos, P.; Taveira-Pinto, F. On the potential synergies and applications of wave energy converters: A review. *Renew. Sustain. Energy Rev.* **2021**, *135*, 110162. [[CrossRef](#)]
3. Guiberteau, K.; Lee, J.; Liu, Y.; Dou, Y.; Kozman, T.A. Wave energy converters and design considerations for gulf of Mexico. *Distrib. Gener. Altern. Energy J.* **2015**, *30*, 55–76.
4. Pastor, J.; Liu, Y. Wave climate resource analysis based on a revised gamma spectrum for wave energy conversion technology. *Sustainability* **2016**, *8*, 1321. [[CrossRef](#)]
5. Guiberteau, K.L.; Liu, Y.; Lee, J.; Kozman, T.A. Investigation of developing wave energy technology in the Gulf of Mexico. *Distrib. Gener. Altern. Energy J.* **2012**, *27*, 36–52.
6. Choupin, O.; Andutta, F.P.; Etemad-Shahidi, A.; Tomlinson, R. A decision-making process for wave energy converter and location pairing. *Renew. Sustain. Energy Rev.* **2021**, *147*, 111225. [[CrossRef](#)]
7. Smith, H.C.; Pearce, C.; Millar, D.L. Further analysis of change in nearshore wave climate due to an offshore wave farm: An enhanced case study for the Wave Hub site. *Renew. Energy* **2012**, *40*, 51–64. [[CrossRef](#)]
8. Luczko, E.; Robertson, B.; Bailey, H.; Hiles, C.; Buckingham, B. Representing non-linear wave energy converters in coastal wave models. *Renew. Energy* **2018**, *118*, 376–385. [[CrossRef](#)]
9. Ruol, P.; Zanuttigh, B.; Martinelli, L.; Kofoed, J.P.; Frigaard, P. Nearshore floating wave energy converters: Applications for coastal protection. In Proceedings of the 32nd International Conference on Coastal Engineering ICCE 2010, Shanghai, China, 30 June–5 July 2010.
10. Nader, J.R.; Fleming, A.; Macfarlane, G.; Penesis, I.; Manasseh, R. Novel experimental modelling of the hydrodynamic interactions of arrays of wave energy converters. *Int. J. Mar. Energy* **2017**, *20*, 109–124. [[CrossRef](#)]
11. Abanades, J.; Greaves, D.; Iglesias, G. Coastal defence using wave farms: The role of farm-to-coast distance. *Renew. Energy* **2015**, *75*, 572–582. [[CrossRef](#)]
12. Tedd, J.; Kofoed, J.P.; Knapp, W.; Friis-Madsen, E.; Sørensen, H.C. Wave Dragon: Prototype wave power production. In Proceedings of the 9th World Renewable Energy Congress: WREC IX, Florence, Italy, 19–25 August 2006; Pergamon Press: Oxford, UK, 2006.
13. Tedd, J.; Kofoed, J.P.; Jasinski, M.; Morris, A.; Friis-Madsen, E.; Wisniewski, R.; Bendtsen, J.D. Advanced control techniques for WEC wave dragon. In Proceedings of the 7th European Wave and Tidal Energy Conference: EWTEC 2007, Porto, Portugal, 11–14 September 2007; European Ocean Energy Association: Brussels, Belgium, 2007.

14. Frigaard, P.; Tedd, J.; Kofoed, J.P.; Friis-Madsen, E. 3 years experience with energy production on the Nissum Bredning Wave Dragon prototype. In Proceedings of the Fourth CA-OE Workshop: Performance Monitoring of Ocean Energy Systems, Lisbon, Portugal, 16–17 November 2006.
15. Moradi, M.; Chertouk, N.; Ilinca, A. Modelling of a wave energy converter impact on coastal erosion, a case study for Palm Beach-Azur, Algeria. *Sustainability* **2022**, *14*, 16595. [[CrossRef](#)]
16. Eskilsson, C.; Palm, J.; Kofoed, J.P.; Friis-Madsen, E. CFD study of the overtopping discharge of the Wave Dragon wave energy converter. In *Renewable Energies Offshore*; CRC Press: Boca Raton, FL, USA, 2015; pp. 287–294.
17. Ahmad, M.F.; Musa, M.A.; Roslan, M.F.; Giap, S.G.E.; Ariffin, E.H.; Eissa, Y.W.S.A.; Salleh, M.H.M.; Alias, F. Study on Wave Overtopping Discharge Affected by Guiding Wall Angle of Wave Dragon Device Using FLOW-3D Software. *J. Adv. Res. Appl. Sci. Eng. Technol.* **2024**, *41*, 208–222.
18. Jafari, M.; Babajani, A.; Hafezisefat, P.; Mirhosseini, M.; Rezania, A.; Rosendahl, L. Numerical simulation of a novel ocean wave energy converter. *Energy Procedia* **2018**, *147*, 474–481. [[CrossRef](#)]
19. Robertson, B. Ocean wave energy generation on the west coast of vancouver island and the queen charlotte islands. *Guelph Eng. J.* **2010**, *3*, 9–18.
20. Iglesias, G.; Carballo, R. Wave farm impact: The role of farm-to-coast distance. *Renew. Energy* **2014**, *69*, 375–385. [[CrossRef](#)]
21. Kofoed, J.P.; Frigaard, P.; Sorenson, H.C.; Friis-Madsen, E. Development of the wave energy converter-Wave Dragon. In Proceedings of the ISOPE International Ocean and Polar Engineering Conference, Seattle, WA, USA, 28 May–2 June 2000; ISOPE: Mountain View, CA, USA, 2000; p. ISOPE-I.
22. Kofoed, J.P.; Frigaard, P.; Friis-Madsen, E.; Sørensen, H.C. Prototype testing of the wave energy converter wave dragon. *Renew. Energy* **2006**, *31*, 181–189. [[CrossRef](#)]
23. Nørgaard, J.H.; Andersen, T.L.; Kofoed, J.P. Wave Dragon Wave Energy Converters Used as Coastal Protection: A physical model test study. In Proceedings of the Coastal Structures 2011: International Conference, Yokohama, Japan, 6–8 September 2011; American Society of Civil Engineers: Reston, VA, USA, 2011; pp. 33–34.
24. Gao, J.; Shi, H.; Zang, J.; Liu, Y. Mechanism analysis on the mitigation of harbor resonance by periodic undulating topography. *Ocean Eng.* **2023**, *281*, 114923. [[CrossRef](#)]
25. Gao, J.; Ma, X.; Zang, J.; Dong, G.; Ma, X.; Zhu, Y.; Zhou, L. Numerical investigation of harbor oscillations induced by focused transient wave groups. *Coast. Eng.* **2020**, *158*, 103670. [[CrossRef](#)]
26. DHI MIKE. *MIKE 21 Spectral Waves FM, Spectral Wave Module User Guide*; DHI Water Environment Health: Hørsholm, Denmark, 2017.
27. Holthuijsen, L.H.; Booij, N.; Herbers, T.H.C. A prediction model for stationary, short-crested waves in shallow water with ambient currents. *Coast. Eng.* **1989**, *13*, 23–54. [[CrossRef](#)]
28. Battjes, J.A.; Janssen, J.P.F.M. Energy Loss and Setup Due to Breaking of Random Waves. In Proceedings of the 16th International Conference on Coastal Engineering, Hamburg, Germany, 27 August–3 September 1978; pp. 569–587. [[CrossRef](#)]
29. Ports and Maritime Organization. *Modeling of Waves in Iranian Seas, Volume One: Caspian Sea*, 1st ed.; Ports and Maritime Organization: London, UK, 1387.
30. Woods Hole Oceanographic Institution. Available online: www.whoi.edu (accessed on 6 May 2024).
31. Soerensen, H.C.; Friis-Madsen, E.; Panhauser, W.; Dunce, D.; Nedkvintne, J.; Frigaard, P.B.; Kofoed, J.P.; Knapp, W.; Riemann, S.; Holmén, E.; et al. Development of wave dragon from scale 1:50 to prototype. In Proceedings of the Fifth European Wave Energy Conference, Cork, Ireland, 27 August–1 September 2003.
32. Gao, J.; Hou, L.; Liu, Y.; Shi, H. Influences of bragg reflection on harbor resonance triggered by irregular wave groups. *Ocean Eng.* **2024**, *305*, 117941. [[CrossRef](#)]
33. Gao, J.; Ma, X.; Dong, G.; Chen, H.; Liu, Q.; Zang, J. Investigation on the effects of Bragg reflection on harbor oscillations. *Coast. Eng.* **2021**, *170*, 103977. [[CrossRef](#)]
34. Moradi, M.; Sajjadi, M.; Balachandar, R.; Arman, A.; Ilinca, A. Experimental analysis of multi-horizontal submerged jets energy dissipater. *ISH J. Hydraul. Eng.* **2022**, *28*, 281–291. [[CrossRef](#)]

Disclaimer/Publisher’s Note: The statements, opinions and data contained in all publications are solely those of the individual author(s) and contributor(s) and not of MDPI and/or the editor(s). MDPI and/or the editor(s) disclaim responsibility for any injury to people or property resulting from any ideas, methods, instructions or products referred to in the content.